

Non-unitary neutrino mixing in short and long-baseline experiments

D. V. Forero,^{1,*} C. Giunti,^{2,†} C. A. Ternes,^{2,‡} and M. Tórtola^{3,§}

¹*Universidad de Medellín, Carrera 87 N° 30 - 65 Medellín, Colombia*

²*Istituto Nazionale di Fisica Nucleare (INFN),*

Sezione di Torino, Via P. Giuria 1, I-10125 Torino, Italy

³*Departament de Física Teòrica, Universitat de València,*

and Instituto de Física Corpuscular,

CSIC-Universitat de València, 46980 Paterna, Spain

Abstract

Non-unitary neutrino mixing in the light neutrino sector is a direct consequence of type-I seesaw neutrino mass models. In these models, light neutrino mixing is described by a sub-matrix of the full lepton mixing matrix and, then, it is not unitary in general. In consequence, neutrino oscillations are characterized by additional parameters, including new sources of CP violation. Here we perform a combined analysis of short and long-baseline neutrino oscillation data in this extended mixing scenario. We did not find a significant deviation from unitary mixing, and the complementary data sets have been used to constrain the non-unitarity parameters. We have also found that the T2K and NOvA tension in the determination of the Dirac CP-phase is not alleviated in the context of non-unitary neutrino mixing.

arXiv:2103.01998v3 [hep-ph] 24 Jul 2021

* dvanegas@udem.edu.co

† carlo.giunti@to.infn.it

‡ ternes@to.infn.it

§ mariam@ific.uv.es

CONTENTS

I. Introduction	2
II. Non-unitary neutrino mixing	3
III. Non-unitary mixing at short-baseline experiments	5
IV. Long-baseline experiments: MINOS/MINOS+, T2K and NOvA	7
V. Bounds on non-unitarity parameters	9
VI. CP violation with non-unitary mixing	11
VII. Conclusions	12
Acknowledgments	13
A. Bounds on the off-diagonal α_{ij} parameters	13
B. Effective oscillation probabilities in SBL and LBL experiments	15
References	16

I. INTRODUCTION

Current neutrino oscillation data [1–3] implies that neutrinos are massive particles. The smallness of the neutrino masses arises naturally in the seesaw mechanism [4–8]. The type-I seesaw mechanism requires the existence of new heavy neutral leptons. In this scenario, lepton mixing has to be extended to account for the new heavy states. Therefore, the 3×3 sub-matrix of the full lepton mixing matrix, that describes the mixing among the light neutrino states, is not unitary anymore. Although the predictions for non-unitarity in high-scale seesaw models are negligible, larger deviations from unitarity are generally expected in low-scale type-I seesaw models, such as the inverse and linear seesaw variants [9–14]. For the case of very heavy neutral leptons, with masses above the electroweak scale, precision and flavour observables can constrain the allowed size of non-unitarity to the per-mille level [15, 16]. Likewise, direct searches for heavy neutral leptons at different experiments set strong limits on the heavy-light mixing for a wide range of masses [17, 18]. Here we will focus on the complementary information on non-unitarity that can be obtained from neutrino experiments. Unfortunately, current neutrino data can only constrain deviations from unitarity up to the percent level [15, 16, 19]. Hopefully, upcoming neutrino experiments will improve the sensitivity to the non-unitarity of the neutrino mixing matrix in the near future [20–24].

Model independent parameterizations of the non-unitary mixing matrix can be obtained under the assumption that the new neutral particles are heavy enough to not be directly produced and, therefore, do not participate in neutrino oscillations [25–27]. A convenient parameterization of the non-unitary submatrix is obtained by multiplying the standard

unitary three-neutrino mixing matrix on the left with a triangular matrix [27]. This parameterization is independent of the number of new particles [27]. Note that, although seesaw mechanisms with relatively light new states [28] could account for the observed short-baseline anomalies [29–40], here we consider only relatively heavy (but still below the electroweak scale) new states, such that the non-unitarity of the mixing matrix is mainly constrained by neutrino oscillation data.

In recent years, lots of efforts have been put to study the effects of a possible deviation from unitarity of three-neutrino mixing [21, 22, 41–51]. In particular, it was shown that the presence of such deviations can affect the sensitivity to standard neutrino oscillation parameters in current and future neutrino experiments [15, 16, 52–56].

In this paper we perform dedicated analyses of short and long-baseline data in presence of non-unitary neutrino mixing. We show that a combined analysis of the data of the short-baseline appearance experiments NOMAD and NuTeV and the long-baseline experiments MINOS/MINOS+, T2K and NOvA allows us to constrain all the non-unitarity parameters.

We also study the effects of the new source of CP violation due to non-unitary mixing on the measurement of the standard CP-violating phase δ in T2K and NOvA [44]. In particular, we investigate if CP violation due to non-unitarity can ease the tension between the measurements of δ in T2K and NOvA [1, 3, 57].

The plan of the paper is as follows: in Section II we summarize the notation used in the paper and provide the expressions of the neutrino oscillation probabilities relevant for our work. In Section III we discuss non-unitary neutrino mixing in short baseline experiments. The main technical details about the long-baseline experiments considered in our analysis are discussed in Section IV. The results of our combined analysis of short and long-baseline data are then discussed in Sections V and VI. Finally, in Section VII we draw our conclusions.

II. NON-UNITARY NEUTRINO MIXING

In type-I seesaw models, which extend the light neutrino sector with several new heavy neutral leptons, the full unitary lepton mixing matrix for 3 light neutrino states and $n - 3$ heavy neutral leptons is

$$U^{n \times n} = \begin{pmatrix} N & S \\ V & T \end{pmatrix}. \quad (1)$$

The $3 \times (n - 3)$ matrix S and the $(n - 3) \times 3$ matrix V describe the mixing between light and heavy states. The $(n - 3) \times (n - 3)$ matrix T contains the mixing among the heavy states, while the mixing among the light neutrino states is given by the 3×3 matrix N , that can be written as [27]

$$N = N^{NP} U = \begin{pmatrix} \alpha_{11} & 0 & 0 \\ \alpha_{21} & \alpha_{22} & 0 \\ \alpha_{31} & \alpha_{32} & \alpha_{33} \end{pmatrix} U. \quad (2)$$

Here, U is the standard unitary three-neutrino mixing matrix. Therefore, all the non-unitary new physics effects are encoded in the triangular matrix N^{NP} , which depends on three real positive diagonal parameters α_{ii} , and three complex parameters α_{ij} ($i \neq j$), which can be decomposed in their moduli $|\alpha_{ij}|$ and their arguments, ϕ_{ij} , which introduce new sources of CP violation.

The non-unitarity parameters can be expressed in terms of the mixing angles of the full matrix $U^{n \times n}$. The diagonal parameters are given by

$$\alpha_{ii} = c_{in} c_{in-1} \dots c_{i4}, \quad (3)$$

where $c_{ij} = \cos \theta_{ij}$ are the cosines of the new mixing angles θ_{ij} of the matrix $U^{n \times n}$ describing the mixing between the light and heavy states. The non-diagonal parameters can be written as

$$\alpha_{21} = c_{2n} c_{2n-1} \dots c_{25} \eta_{24} \bar{\eta}_{14} + c_{2n} \dots c_{26} \eta_{25} \bar{\eta}_{15} c_{14} + \dots + \eta_{2n} \bar{\eta}_{1n} c_{1n-1} \dots c_{14}, \quad (4)$$

$$\alpha_{32} = c_{3n} c_{3n-1} \dots c_{35} \eta_{34} \bar{\eta}_{24} + c_{3n} \dots c_{36} \eta_{35} \bar{\eta}_{25} c_{24} + \dots + \eta_{3n} \bar{\eta}_{2n} c_{2n-1} \dots c_{24}, \quad (5)$$

$$\alpha_{31} = c_{3n} c_{3n-1} \dots c_{35} \eta_{34} c_{24} \bar{\eta}_{14} + c_{3n} \dots c_{36} \eta_{35} c_{25} \bar{\eta}_{15} c_{14} + \dots + \eta_{3n} c_{2n} \bar{\eta}_{1n} c_{1n-1} \dots c_{14}, \quad (6)$$

with $\eta_{ij} = \sin \theta_{ij} e^{-i\delta_{ij}}$, where δ_{ij} is the CP phase associated to the angle θ_{ij} (not to be confused with $\phi_{ij} = \arg(\alpha_{ij})$, which in general depend on these δ 's). The non-diagonal parameters are related to the diagonal ones through the triangular inequality [16] (see Appendix A)

$$|\alpha_{ij}| \leq \sqrt{(1 - \alpha_{ii}^2)(1 - \alpha_{jj}^2)}. \quad (7)$$

In the following, we briefly review the oscillation probabilities relevant for the experiments discussed in this paper. The general expression for the neutrino oscillation probability in the $\nu_\alpha \rightarrow \nu_\beta$ channel is given by

$$P_{\alpha\beta} = |(NN^\dagger)_{\alpha\beta}|^2 - 4 \sum_{k>j} \Re [N_{\alpha k}^* N_{\beta k} N_{\alpha j} N_{\beta j}^*] \sin^2 \left(\frac{\Delta m_{kj}^2 L}{4E} \right) + 2 \sum_{k>j} \Im [N_{\alpha k}^* N_{\beta k} N_{\alpha j} N_{\beta j}^*] \sin \left(\frac{\Delta m_{kj}^2 L}{2E} \right). \quad (8)$$

Note that the first term of the probability is not equal to $\delta_{\alpha\beta}$ as in the unitary case (it depends only on the values of the α parameters, as one can see from Eq. (A5) in Appendix A). This means that, in presence of non-unitary neutrino mixing, a zero-distance flavor conversion is possible. Apart from this, the neutrino oscillation probability has the same structure as in the standard case with U replaced by N . In what follows, we drop terms which are cubic products of the ‘‘small’’ parameters $\sin \theta_{13}$, $\Delta m_{21}^2 / \Delta m_{31}^2$ and $|\alpha_{21}|$. In this approximation, the vacuum ν_μ disappearance probability in presence of non-unitarity is given by [27]

$$P_{\mu\mu} = \alpha_{22}^4 P_{\mu\mu}^{\text{st}} + \alpha_{22}^3 |\alpha_{21}| P_{\mu\mu}^{I_1} + 2 |\alpha_{21}|^2 \alpha_{22}^2 P_{\mu\mu}^{I_2}, \quad (9)$$

where $P_{\mu\mu}^{\text{st}}$ is the standard unitary oscillation probability in vacuum and the new terms are given by

$$P_{\mu\mu}^{I_1} = -8 \sin \theta_{13} \sin \theta_{23} \cos 2\theta_{23} \cos(\delta - \phi_{21}) \sin^2 \left(\frac{\Delta m_{31}^2 L}{4E} \right) \quad (10)$$

$$+ 2 \cos \theta_{23} \sin 2\theta_{12} \sin^2 \theta_{23} \cos \phi_{21} \sin \left(\frac{\Delta m_{31}^2 L}{2E} \right) \sin \left(\frac{\Delta m_{21}^2 L}{2E} \right) \quad (11)$$

and

$$P_{\mu\mu}^{I_2} = 1 - 2 \sin^2 \theta_{23} \sin^2 \left(\frac{\Delta m_{31}^2 L}{4E} \right). \quad (12)$$

The $\nu_\mu \rightarrow \nu_e$ appearance probability is given by

$$P_{\mu e} = (\alpha_{11}\alpha_{22})^2 P_{\mu e}^{\text{st}} + \alpha_{11}^2 \alpha_{22} |\alpha_{21}| P_{\mu e}^I + \alpha_{11}^2 |\alpha_{21}|^2. \quad (13)$$

Again, $P_{\mu e}^{\text{st}}$ is the standard unitary oscillation probability and the new term is given by

$$P_{\mu e}^I = -2 \left[\sin 2\theta_{13} \sin \theta_{23} \sin \left(\frac{\Delta m_{31}^2 L}{4E_\nu} \right) \sin \left(\frac{\Delta m_{31}^2 L}{4E_\nu} + \delta - \phi_{21} \right) \right] \\ + \cos \theta_{13} \cos \theta_{23} \sin 2\theta_{12} \sin \phi_{21} \sin \left(\frac{\Delta m_{21}^2 L}{2E_\nu} \right). \quad (14)$$

In addition to the standard parameters, the oscillation probabilities under consideration depend on α_{22} , α_{11} , $|\alpha_{21}|$ and ϕ_{21} . The remaining non-unitarity parameters contribute only through matter effects [15, 16] to the oscillation probabilities considered here.

It should be noted that, in many experiments, the spectrum at a far detector is inferred from the measured spectrum at a near detector. In this case, the oscillation probability needs to be corrected including the non-unitary effects which have already occurred at very short distances. This becomes important in the analysis of several of the experiments considered here, see Appendix B.

Let us also remind that one can translate parameters characterizing non-unitarity in terms of other parameterizations, such as the one defining the light mixing matrix as $N = (\mathbf{1} - \eta) U$ [25, 45] that is often used to study the effects of non-unitary neutrino mixing. In this parameterization, η is a Hermitian 3×3 matrix that describes the unitarity violations. Comparing the expressions of NN^\dagger in the two parameterizations, one can find that, at first order of the η parameters, $\alpha_{11}^2 \simeq 1 - 2\eta_{ee}$, $\alpha_{11}\alpha_{21}^* \simeq -2\eta_{e\mu}$, and $\alpha_{22}^2 + |\alpha_{21}|^2 \simeq 1 - 2\eta_{\mu\mu}$. Therefore, for small unitarity violations, we have the direct approximate relations $\alpha_{ii} \simeq 1 - \eta_{ii}$ and $\alpha_{21}^* \simeq -2\eta_{e\mu}$.

III. NON-UNITARY MIXING AT SHORT-BASELINE EXPERIMENTS

In this section we discuss the effects of non-unitarity in short-baseline (SBL) $\nu_\mu \rightarrow \nu_e$ and $\bar{\nu}_\mu \rightarrow \bar{\nu}_e$ oscillation experiments and we derive the most stringent bounds on the non-unitarity parameters that can be obtained from the current data. We consider only these channels because other channels, that have been considered in Ref. [16], give less stringent bounds on the non-unitarity parameters that are relevant for the combined analysis with the data of long-baseline experiments discussed in Section V.

Considering that in the analysis of the data of short-baseline experiments $P_{\mu e}^{\text{st}}$ and $P_{\mu e}^I$ in Eq. (13) are negligible, the effective probability of $\nu_\mu \rightarrow \nu_e$ and $\bar{\nu}_\mu \rightarrow \bar{\nu}_e$ transitions takes the very simple form

$$P_{\mu e}^{\text{SBL}} = \alpha_{11}^2 |\alpha_{21}|^2. \quad (15)$$

Therefore, short-baseline experiments are only sensitive to the energy-independent zero-distance effect coming from the first term in Eq. (8).

There are several short-baseline $\nu_\mu \rightarrow \nu_e$ and $\bar{\nu}_\mu \rightarrow \bar{\nu}_e$ oscillation experiments that did not find any indication in favor of these transitions. The data were analyzed using the standard unitary two-neutrino mixing approximation, where the transition probability depends on the mixing parameter $\sin^2 2\vartheta$ and the squared-mass difference Δm^2 . In this case, for large values of Δm^2 , oscillations are averaged and the oscillation probability is simply equal to

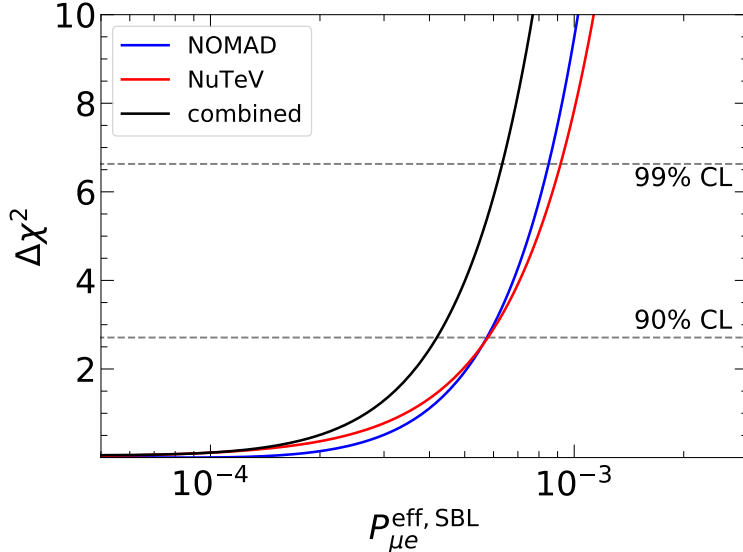


FIG. 1. $\Delta\chi^2$ profiles obtained from our analysis of NOMAD (blue line) and NuTeV (red line) data and from the combination of the two data sets (black line).

$\sin^2 2\vartheta/2$. Therefore, it is possible to obtain the bound on the probability $P_{\mu e}^{\text{SBL}}$ in each of these short-baseline experiments from the value of the χ^2 as a function of $\sin^2 2\vartheta$ at a sufficiently large fixed value of Δm^2 . Such bounds on $P_{\mu e}^{\text{SBL}}$ can be used to constrain the non-unitarity parameters through Eq. (15).

In the following we consider the short-baseline experiments NOMAD [58] and NuTeV [59], that give the most stringent bounds on $P_{\mu e}^{\text{SBL}}$.

NOMAD was actually an experiment designed to search for short-baseline $\nu_\mu \rightarrow \nu_\tau$ appearance. However, due to the good electron identification efficiency, it could also be used to look for short-baseline ν_e appearance from a ν_μ beam through the charged current reaction $\nu_e + N \rightarrow e^- + X$. NOMAD collected data from 1995 to 1998, running principally in neutrino mode. The exposure corresponds to 5.1×10^{19} protons on target (POT) in neutrino mode and only 0.44×10^{19} in antineutrino mode. They did not find any evidence of $\nu_\mu \rightarrow \nu_e$ oscillations.

Also the NuTeV collaboration performed a search for short-baseline $\nu_\mu \rightarrow \nu_e$ and $\bar{\nu}_\mu \rightarrow \bar{\nu}_e$ appearance. NuTeV used the 800 GeV proton beam from Tevatron and collected data in the time period of 1996-1997. The usage of focusing magnets allowed for separate analyses of $\nu_\mu \rightarrow \nu_e$ and $\bar{\nu}_\mu \rightarrow \bar{\nu}_e$. No evidence of appearance was found for either oscillation channel. Here we use the results from the combined analysis of neutrino and antineutrino oscillation channels.

Note that, in the two experiments described above, the appearance signal is inferred from the ν_μ -disappearance spectrum. Therefore, the effective oscillation probability measured by these experiments is given by (see Eq. (B5) in Appendix B)

$$P_{\mu e}^{\text{eff, SBL}} = \frac{\alpha_{11}^2 |\alpha_{21}|^2}{(\alpha_{22}^2 + |\alpha_{21}|^2)^2}, \quad (16)$$

instead of Eq. (15).

The bounds that can be obtained from the short-baseline NOMAD and NuTeV data are shown in Fig. 1. The blue (red) lines correspond to NOMAD (NuTeV) data, while

the black line is obtained from the combination of both experiments. Note that short-baseline experiments cannot constrain any of the α_{ij} parameters independently, but only the combination of them which determines the observable transition probability in Eq. (16). We find that both experiments have similar sensitivities to the zero-distance appearance probability, obtaining $P_{\mu e}^{\text{eff,SBL}} < 6 \times 10^{-4}$ at 90% C.L., while the combined bound is $P_{\mu e}^{\text{eff,SBL}} < 4 \times 10^{-4}$ (6×10^{-4}) at 90% (99%) C.L. In Section V we will combine short-baseline and long-baseline neutrino data to improve the sensitivity on the non-unitary mixing. This combination can be easily done by transforming the χ^2 results in terms of $P_{\mu e}$, as plotted in Fig. 1, to a χ^2 function depending on α_{11} , $|\alpha_{21}|$ and α_{22} using Eq. (16).

We considered also the NOMAD [60] bounds on short-baseline $\nu_\mu \rightarrow \nu_\tau$ and $\nu_e \rightarrow \nu_\tau$ transitions*, that allow us to constrain the non-unitarity parameters $|\alpha_{31}|$ and $|\alpha_{32}|$. Since the NOMAD signal prediction was obtained correcting the Monte Carlo by using a sample of ν_μ charged-current events from the data [60], in analogy with Eq. (B5) in Appendix B, the effective oscillation probabilities are given by

$$P_{\mu\tau}^{\text{eff,SBL}} = \frac{|\alpha_{22}\alpha_{32}^* + \alpha_{21}\alpha_{31}^*|^2}{(\alpha_{22}^2 + |\alpha_{21}|^2)^2} \geq \frac{(\alpha_{22}|\alpha_{32}| - |\alpha_{21}||\alpha_{31}|)^2}{(\alpha_{22}^2 + |\alpha_{21}|^2)^2}, \quad (17)$$

$$P_{e\tau}^{\text{eff,SBL}} = \frac{\alpha_{11}^2 |\alpha_{31}|^2}{(\alpha_{22}^2 + |\alpha_{21}|^2)^2}. \quad (18)$$

Unfortunately, the very complicated analysis of the NOMAD data presented in Ref. [60] cannot be reproduced outside of the NOMAD collaboration. Therefore, we considered an approximate χ^2 obtained with a linear interpolation of the bounds published in Ref. [60].

IV. LONG-BASELINE EXPERIMENTS: MINOS/MINOS+, T2K AND NOVA

As we showed in Section II, if the light neutrino mixing matrix is not unitary, new correlations arise among the standard oscillation parameters and the parameters characterizing non-unitarity. We use the MINOS/MINOS+ data sample from Ref. [62] as well as the most recent data from the long-baseline (LBL) experiments T2K [63] and NOvA [64] to search for deviations from unitarity.

The Main Injector Neutrino Oscillation Search (MINOS) is an accelerator-based neutrino oscillation experiment studying muon neutrinos produced by the NuMI beam facility at Fermilab and detected at the far (near) detector located at 735 km (1.04 km) from the source. During the MINOS data taking period, the neutrino beam peaked at an energy of 3 GeV. Later, the beam was tuned to cover larger energies, with an energy peak at 7 GeV, for the upgraded version of the experiment, MINOS+. Here we consider data corresponding to an exposure of 10.56×10^{20} POT in MINOS (mostly in neutrino mode, only 3.36×10^{20} POT were gathered in antineutrino mode) and 5.80×10^{20} POT in MINOS+ (in neutrino mode), collected in the same detectors [62].

The T2K collaboration observed events induced by neutrinos and antineutrinos, corresponding to an exposure at Super-Kamiokande of 1.97×10^{21} POT in neutrino mode and 1.63×10^{21} POT in antineutrino mode. T2K observed 318 (137) muon (anti-muon) events and 94 (16) electron (positron) events. In addition, 14 electron events with an associated

* For simplicity, we neglected the weaker limits obtained in the contemporary CHORUS experiment [61] and in other previous experiments.

pion were recorded. These results allowed the T2K collaboration to exclude CP-conserving values of δ at about 2σ confidence level [65].

NOvA has reached 13.6×10^{20} POT in neutrino mode [66] and 12.5×10^{20} POT in antineutrino mode, observing 212 (105) muon (anti-muon) events and 82 (33) electron (positron) events. Unlike T2K, the latest NOvA neutrino and antineutrino data prefer values of the CP-violating phase δ close to 0.8π , in tension with the T2K result.

The most recent T2K and NOvA data as well as the relevant technical information have been extracted from Refs. [65] and [64], respectively. For the energy reconstruction we assume Gaussian smearing adding bin-to-bin efficiencies, which are adjusted to reproduce the best-fit spectra reported by the experimental collaborations. Our statistical analysis includes several sources of systematic uncertainties, related to the signal and background predictions. We perform the analysis of the experimental data using GLOBES [67, 68] in combination with a package which calculates the oscillation probabilities in matter in presence of non-unitary neutrino mixing, developed for the analysis in Ref. [16]. Since the spectra at the far detectors of T2K and NOvA are inferred from the measured spectra at their near detectors, the effective appearance and disappearance oscillation probabilities relevant for these experiments need to be corrected due to zero distance effects at the near detector, see Appendix B. Substituting Eq. (9) into Eq. (B4), we obtain the effective disappearance probability in T2K and NOvA

$$P_{\mu\mu}^{\text{eff,LBL}} = \frac{\alpha_{22}^4 P_{\mu\mu}^{\text{st}} + \alpha_{22}^3 |\alpha_{21}| P_{\mu\mu}^{I_1} + 2|\alpha_{21}|^2 \alpha_{22}^2 P_{\mu\mu}^{I_2}}{(\alpha_{22}^2 + |\alpha_{21}|^2)^2}. \quad (19)$$

Since $|\alpha_{21}|$ is small, the leading dependence on α_{22} of the first term in the numerator is practically cancelled by the denominator. Therefore, T2K and NOvA can not set strong constraints on α_{22} . Likewise, the bounds on $|\alpha_{21}|$ are weak and not competitive with that of SBL experiments discussed in Section III. However, this ensures that the measurement of the standard oscillation parameters is robust in the presence of non-unitarity.

In the case of MINOS/MINOS+ [62], we adopted the analysis procedure followed by the experimental collaboration for the search of active-sterile neutrino oscillations in Ref. [62]. We adapted the public MINOS/MINOS+ code to account for non-unitary neutrino oscillations, instead of active-sterile oscillations. In this code, the spectra at both detectors are fitted simultaneously assuming the MINERvA flux prediction [69], that was obtained with hadronic data and, hence, is independent of neutrino mixing. Therefore, the analysis of the MINOS/MINOS+ data sample is sensitive to the zero-distance effect and allows us to put stringent bounds on the non-unitarity parameters.

Another difference with respect to the analysis of T2K and NOvA is that, in the analysis of MINOS/MINOS+ data, NC events are considered in addition to CC events. The NC sample is sensitive to the following sum of the muon neutrino survival probability plus the electron and tau neutrino appearance probabilities, which deviates from unity in the case of non-unitarity (and active-sterile) mixing:

$$P_{\mu}^{\text{NC}} = \sum_{\alpha=e,\mu,\tau} P_{\mu\alpha} \approx [(\alpha_{11}\alpha_{22})^2 P_{\mu e}^{\text{st}} + \alpha_{22}^4 P_{\mu\mu}^{\text{st}} + (\alpha_{22}\alpha_{33})^2 P_{\mu\tau}^{\text{st}}], \quad (20)$$

where we have considered only the dominant effects of the diagonal non-unitarity parameters, and $P_{\mu\alpha}^{\text{st}}$ is the standard probability of $\nu_{\mu} \rightarrow \nu_{\alpha}$ transitions in the unitary three-neutrino mixing scenario (with $\sum_{\alpha=e,\mu,\tau} P_{\mu\alpha}^{\text{st}} = 1$). Equation (20) shows that the analysis of MINOS/MINOS+ NC events can constrain all the tree diagonal α 's, but since α_{11} and α_{22} are

better constrained by MINOS/MINOS+ CC and other data, the NC analysis is mainly relevant for constraining α_{33} . Moreover, using the inequality in Eq. (7), one can also constrain $|\alpha_{31}|$ and $|\alpha_{32}|$. Therefore, the analysis of the full MINOS/MINOS+ data sample allows us to fully constrain the non-unitarity of the light neutrino mixing matrix.

V. BOUNDS ON NON-UNITARITY PARAMETERS

In this section we present the results of our combined analysis of short and long-baseline data in the presence of non-unitary neutrino mixing. In the context of long-baseline neutrino oscillations, many new parameters have to be considered in the analysis. Regarding the standard parameters, we keep the reactor mixing angle and the solar parameters fixed at $\sin^2 \theta_{13} = 0.022$, $\sin^2 \theta_{12} = 0.318$ and $\Delta m_{21}^2 = 7.5 \times 10^{-5} \text{ eV}^2$, respectively [1]. We have checked that fixing the reactor angle or minimizing over it within its allowed 3σ -range has no effect on the results of the current analysis. It is sufficient to consider the range determined from the unitary fit of reactor data because the ν_e survival probability at reactor experiments is simply given by $P_{ee} = \alpha_{11}^4 P_{ee}^{\text{st}}$ [27]. Therefore, the factor α_{11}^4 basically takes the role of a new flux normalization and the measurement of θ_{13} using event ratios from detectors at different baselines (as done by the current reactor experiments) is robust under non-unitary deviations of neutrino mixing. The solar parameters play only a minor role in the context of the long-baseline experiments considered here and can be safely kept fixed at their best fit values. Regarding the non-unitarity parameters, those associated to the third row of the non-unitarity matrix N^{NP} , α_{3i} , enter the oscillation probabilities relevant for T2K and NOvA only via matter effects and their effect is very small, as shown in Ref. [16]. However, they can be accessed in MINOS/MINOS+ through neutral current events. The remaining parameters ($\sin^2 \theta_{23}$, Δm_{31}^2 , δ , α_{22} , α_{11} , $|\alpha_{21}|$ and ϕ_{21}) are varied freely in the analysis of all experiments. In the case of MINOS/MINOS+, we also vary α_{33} , that can be measured through the NC events, which are not included in the analyses of NOvA and T2K data. Using the relation in Eq. (7) we can also bound the off-diagonal parameters, α_{3i} [†].

Since T2K and NOvA show a limited sensitivity to the non-unitarity parameters, we start the analysis with MINOS/MINOS+ data and then subsequently add short-baseline results and next T2K and NOvA data. In Fig. 2 we show the sensitivity to different non-unitarity parameters from the analysis of MINOS/MINOS+, MINOS/MINOS+ plus short-baseline experiments and the combination of all data samples. It should be noted that MINOS/MINOS+ on its own can put strong limits on non-unitarity (see the green lines in Fig. 2). Notice as well that the bound on $|\alpha_{21}|$ from MINOS/MINOS+ does not come from the $\nu_\mu \rightarrow \nu_e$ appearance channel, which has very small statistics, but from the combined constraints on α_{11} and α_{22} and the use of the inequality in Eq. (7). The addition of short-baseline data (see the black lines in Fig. 2) has very little impact on the sensitivity to the diagonal parameters α_{11} and α_{22} , but improves the bound on $|\alpha_{21}|$. After combining with the data from T2K and NOvA (see the magenta lines in Fig. 2), the volumes of the allowed regions further shrink, since degeneracies among non-unitarity and standard oscillation parameters break, thanks to the better determination of the standard parameters in T2K and NOvA in comparison with MINOS/MINOS+.

Figure 3 shows the marginal $\Delta\chi^2$ profiles for the diagonal (left) and off-diagonal (right) non-unitarity parameters obtained from the combination of all the data discussed above.

[†] We verified that the sensitivity to these parameters comes exclusively from Eq. (7).

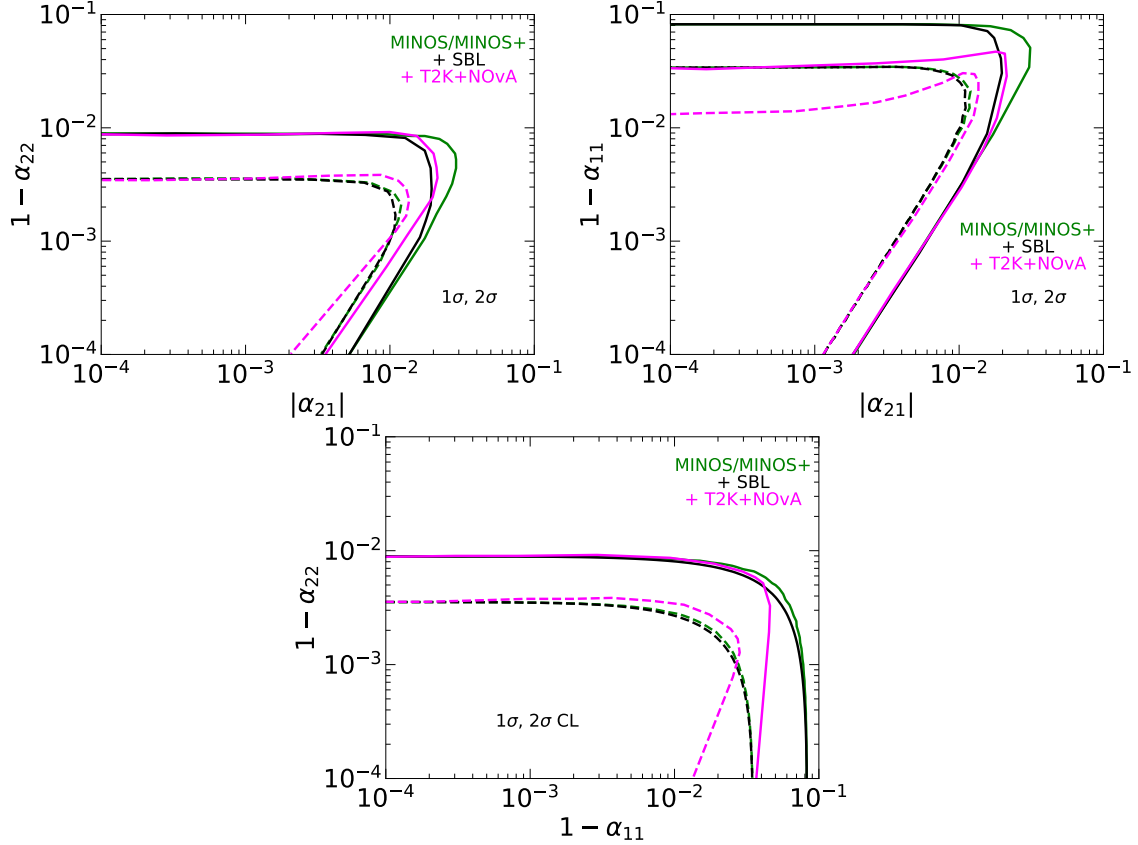


FIG. 2. 1σ (dashed) and 2σ (solid) allowed regions in three planes of the non-unitarity parameters obtained from our analysis of MINOS/MINOS+ data (green), in combination with short-baseline oscillation data (black), and after combining with T2K and NOvA data too (magenta).

The corresponding 90% and 99% C.L. limits are summarized in Tab. I. Note that some of the constraints on the non-unitarity parameters, particularly on $|\alpha_{21}|$, are slightly weaker than those in Refs. [15, 16, 49]. This is due to the use of additional data beyond short and long-baseline results in those references and also to the consideration of the denominator in the effective short-baseline oscillation probability, Eq. (16), in our current work. However, the analysis of the MINOS/MINOS+ data assuming the MINERvA flux prediction [69] allowed us to improve significantly the bound on $1 - \alpha_{22}$, that is about twice as strong as in previous analyses [15, 16].

As discussed at the end of Section IV, the analysis of MINOS/MINOS+ neutral current data allows us to constrain α_{33} and, through the inequality (7), also $|\alpha_{31}|$ and $|\alpha_{32}|$. Moreover, in the global analysis of short-baseline and long-baseline data, we also considered the NOMAD bounds on the non-diagonal parameters $|\alpha_{31}|$ and $|\alpha_{32}|$ discussed at the end of Section III. These results contribute significantly to the improvement of the global bounds on the non-unitarity parameters, especially for $|\alpha_{32}|$.

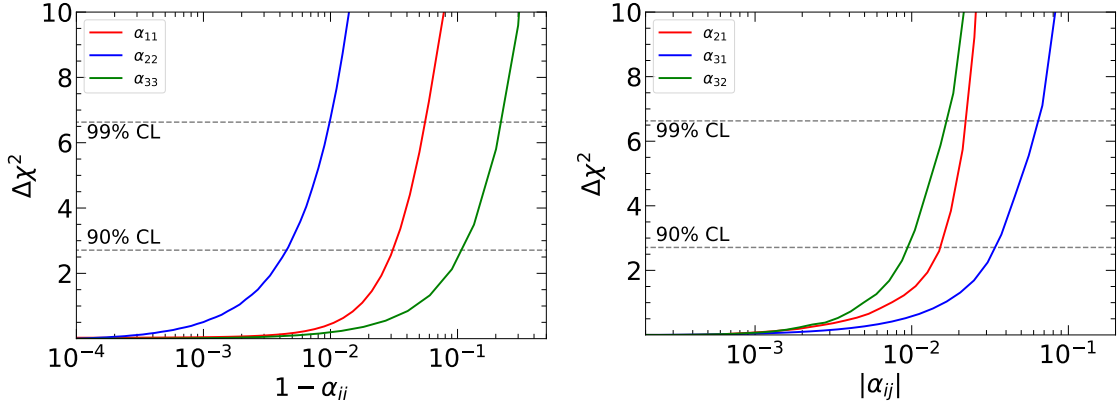


FIG. 3. $\Delta\chi^2$ profiles for the diagonal (left) and non-diagonal (right) non-unitarity parameters obtained from the combined analysis of short and long-baseline neutrino oscillation data.

Parameter	90% C.L.	99% C.L.
$1 - \alpha_{11}$	< 0.031	< 0.056
$1 - \alpha_{22}$	< 0.005	< 0.010
$1 - \alpha_{33}$	< 0.110	< 0.220
$ \alpha_{21} $	< 0.013	< 0.023
$ \alpha_{31} $	< 0.033	< 0.065
$ \alpha_{32} $	< 0.009	< 0.017

TABLE I. Bounds on the non-unitarity parameters obtained in this analysis.

VI. CP VIOLATION WITH NON-UNITARY MIXING

Let us now consider the measurement of CP violation in the T2K and NOvA long-baseline experiments with the aim of investigating if the effects of non-unitary mixing can resolve the tension between the data of the two experiments [1, 3, 57] in the case of a normal neutrino mass ordering. The relevant CP violating phases are the standard Dirac CP phase δ and the argument of the non-unitarity parameter α_{21} , ϕ_{21} . Figure 4 shows the 1σ allowed regions in the ϕ_{21} - δ plane obtained from the analysis of T2K (blue regions) and NOvA (red regions) by considering two sets of fixed values of the non-unitarity parameters α_{11} , α_{22} , and $|\alpha_{21}|$. The first set of non-unitarity parameters (left panel) corresponds to a benchmark point well within the 90% C.L. bounds in Tab. I, while the second set (right panel) corresponds to a choice at the borders of the 90% and 99% C.L. limits for α_{11} and α_{22} , respectively, and near the border of the 99% C.L. bound for $|\alpha_{21}|$. As one can see, in both cases the 1σ T2K and NOvA allowed regions are almost completely disjoint, as in the unitary case. These two examples illustrate our general finding: the overlap of the regions allowed by T2K and NOvA does not become significant for any combination of the α_{ij} parameters that is allowed by the data. Therefore, we conclude that, differently to what happens with other new physics scenarios [70–72], the non-unitarity of the neutrino mixing matrix cannot reduce the tension between the T2K and NOvA measurements of the CP phase δ in the case of a normal neutrino mass ordering.

Let us remark that an analysis similar to that presented here has been performed in

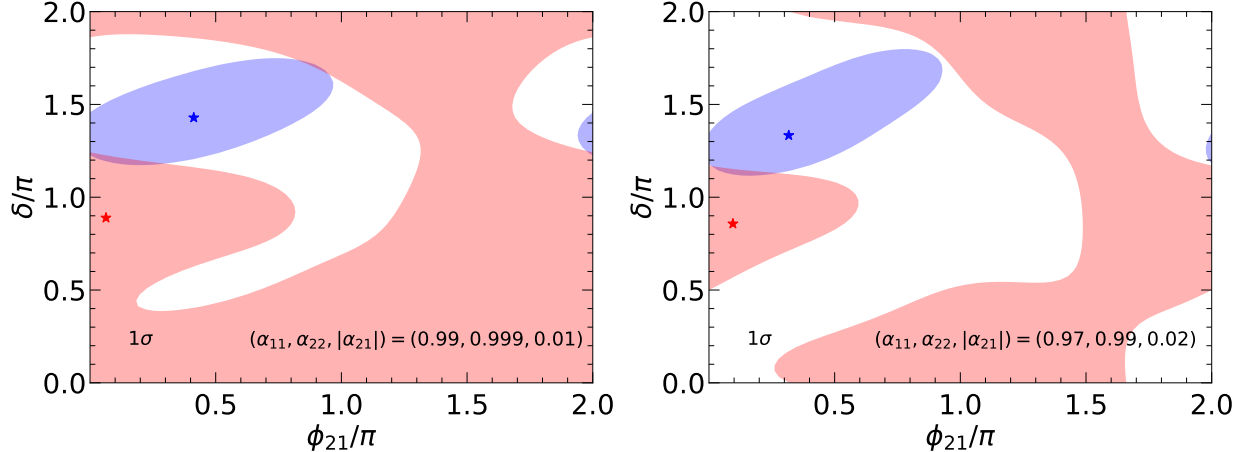


FIG. 4. 1σ allowed regions in the (ϕ_{21}, δ) plane obtained from the analysis of T2K (blue regions) and NOvA (red regions). The stars indicate the corresponding best fit points. In each panel we fix α_{11} , α_{22} and $|\alpha_{21}|$ to the indicated values.

Ref. [56]. The authors considered only T2K and NOvA data and obtained a preference for large deviations from unitarity, which are excluded in our analysis. In particular, we find that their best fit values, $\alpha_{11} = 0.7$ and $|\alpha_{21}| = 0.125$, are disfavored with very large significance, as it can be seen from Fig. 3. This shows the great impact of short-baseline and MINOS/MINOS+ data in the analysis of non-unitarity in the neutrino mixing.

VII. CONCLUSIONS

The non-unitarity of the light-neutrino mixing matrix is a direct consequence of the celebrated seesaw mechanism. Therefore, analyses testing its consequences or predictions are very important for the hunt of new physics. Here we present an analysis of short and long-baseline neutrino oscillation data in the presence of non-unitary neutrino mixing. We have found that neutrino oscillation experiments can bound some of the non-unitarity parameters at appreciable level. Our main results are summarized in Fig. 3 and Tab. I. Most of the bounds derived on the different non-unitarity parameters are comparable in size with the ones in literature [15, 16]. However, we can highlight a large improvement in the constraint on $1 - \alpha_{22}$, which improves previous limits at least by a factor of 2. Although these results have been obtained from a combination of neutrino oscillation experiments, the largest sensitivity to non-unitarity comes from the analysis of MINOS/MINOS+ data, as shown in Fig. 2.

We also investigated the effects of the new CP-violating phase ϕ_{21} on the determination of the standard CP-violating phase δ in the T2K and NOvA experiments. In particular, we have shown that the new source of CP-violation due to non-unitarity cannot decrease the current tension between T2K and NOvA in the determination of δ .

ACKNOWLEDGMENTS

We would like to thank Stephen Parke for useful comments on the first version of this manuscript. CG and CAT are supported by the research grant ‘‘The Dark Universe: A Synergic Multimessenger Approach’’ number 2017X7X85K under the program ‘‘PRIN 2017’’ funded by the Ministero dell’Istruzione, Universita e della Ricerca (MIUR). MT is supported by the Spanish grants FPA2017-85216-P (AEI/FEDER, UE), PROMETEO/2018/165 (Generalitat Valenciana) and the Spanish Red Consolider MultiDark FPA2017-90566-REDC.

Appendix A: Bounds on the off-diagonal α_{ij} parameters

In this Appendix we present the proof of the validity of the inequalities (7) for any value of the mixing. These inequalities were obtained in Ref. [16], where they have been proved assuming small unitarity violation.

Considering the full $n \times n$ unitary matrix $U^{n \times n}$ in Eq. (1), we have the unitary relations

$$\sum_{k=1}^3 U_{\alpha k}^{n \times n} U_{\beta k}^{n \times n*} + \sum_{k=4}^N U_{\alpha k}^{n \times n} U_{\beta k}^{n \times n*} = \delta_{\alpha\beta}, \quad (\text{A1})$$

that for $\alpha \neq \beta$ imply

$$\left| \sum_{k=1}^3 U_{\alpha k}^{n \times n} U_{\beta k}^{n \times n*} \right|^2 = \left| \sum_{k=4}^N U_{\alpha k}^{n \times n} U_{\beta k}^{n \times n*} \right|^2. \quad (\text{A2})$$

Applying the Cauchy-Schwarz inequality to the right-hand side of (A2) and using the unitarity relation (A1) for $\alpha = \beta$, we obtain

$$\begin{aligned} \left| \sum_{k=1}^3 U_{\alpha k}^{n \times n} U_{\beta k}^{n \times n*} \right|^2 &\leq \left(\sum_{k=4}^N |U_{\alpha k}^{n \times n}|^2 \right) \left(\sum_{k=4}^N |U_{\beta k}^{n \times n}|^2 \right) \\ &= \left(1 - \sum_{k=1}^3 |U_{\alpha k}^{n \times n}|^2 \right) \left(1 - \sum_{k=1}^3 |U_{\beta k}^{n \times n}|^2 \right). \end{aligned} \quad (\text{A3})$$

Considering the truncated 3×3 nonunitary submatrix of $U^{n \times n}$, N , the bound (A3) reads

$$|(NN^\dagger)_{\alpha\beta}|^2 \leq (1 - (NN^\dagger)_{\alpha\alpha}) (1 - (NN^\dagger)_{\beta\beta}). \quad (\text{A4})$$

In terms of the parameterization (2) of N , the matrix NN^\dagger is given by

$$NN^\dagger = \begin{pmatrix} \alpha_{11}^2 & \alpha_{11}\alpha_{21}^* & \alpha_{11}\alpha_{31}^* \\ \alpha_{11}\alpha_{21} & \alpha_{22}^2 + |\alpha_{21}|^2 & \alpha_{22}\alpha_{32}^* + \alpha_{21}\alpha_{31}^* \\ \alpha_{11}\alpha_{31} & \alpha_{22}\alpha_{32} + \alpha_{21}^*\alpha_{31} & \alpha_{33}^2 + |\alpha_{31}|^2 + |\alpha_{32}|^2 \end{pmatrix}. \quad (\text{A5})$$

Therefore, we have the following three inequalities:

1. From $|(NN^\dagger)_{e\mu}|^2 \leq (1 - (NN^\dagger)_{ee}) (1 - (NN^\dagger)_{\mu\mu})$ we have

$$\alpha_{11}^2 |\alpha_{21}|^2 \leq (1 - \alpha_{11}^2) (1 - \alpha_{22}^2 - |\alpha_{21}|^2). \quad (\text{A6})$$

Then, it is straightforward to obtain the inequality (7) for $|\alpha_{21}|$.

2. $|(NN^\dagger)_{e\tau}|^2 \leq (1 - (NN^\dagger)_{ee}) (1 - (NN^\dagger)_{\tau\tau})$ implies that

$$\alpha_{11}^2 |\alpha_{31}|^2 \leq (1 - \alpha_{11}^2) (1 - \alpha_{33}^2 - |\alpha_{31}|^2 - |\alpha_{32}|^2). \quad (\text{A7})$$

Therefore,

$$|\alpha_{31}|^2 \leq (1 - \alpha_{11}^2) (1 - \alpha_{33}^2 - |\alpha_{32}|^2). \quad (\text{A8})$$

The obvious inequality $(1 - \alpha_{33}^2 - |\alpha_{32}|^2) \leq (1 - \alpha_{33}^2)$ leads to the weaker constraint (7) for $|\alpha_{31}|$.

3. $|(NN^\dagger)_{\mu\tau}|^2 \leq (1 - (NN^\dagger)_{\mu\mu}) (1 - (NN^\dagger)_{\tau\tau})$ implies that

$$|\alpha_{22}\alpha_{32} + \alpha_{21}^* \alpha_{31}|^2 \leq (1 - \alpha_{22}^2 - |\alpha_{21}|^2) (1 - \alpha_{33}^2 - |\alpha_{31}|^2 - |\alpha_{32}|^2). \quad (\text{A9})$$

This case is more complicated. Since

$$|\alpha_{22}\alpha_{32} + \alpha_{21}^* \alpha_{31}|^2 \geq (|\alpha_{22}||\alpha_{32}| - |\alpha_{21}||\alpha_{31}|)^2, \quad (\text{A10})$$

there are two cases that need to be considered:

(a) $|\alpha_{22}||\alpha_{32}| \leq |\alpha_{21}||\alpha_{31}|$. In this case there is not even need of the inequality (A9), because from the inequalities (7) for $|\alpha_{21}|$ and $|\alpha_{31}|$ we have

$$\begin{aligned} \alpha_{22}^2 |\alpha_{32}|^2 &\leq (1 - \alpha_{11}^2)^2 (1 - \alpha_{22}^2) (1 - \alpha_{33}^2 - |\alpha_{32}|^2) \\ &\leq (1 - \alpha_{22}^2) (1 - \alpha_{33}^2 - |\alpha_{32}|^2), \end{aligned} \quad (\text{A11})$$

that gives the inequality (7) for $|\alpha_{32}|$.

(b) $|\alpha_{22}||\alpha_{32}| > |\alpha_{21}||\alpha_{31}|$. In this case, we have

$$|\alpha_{22}\alpha_{32} + \alpha_{21}^* \alpha_{31}| \geq |\alpha_{22}||\alpha_{32}| - |\alpha_{21}||\alpha_{31}|. \quad (\text{A12})$$

Therefore, from (A9) we obtain

$$|\alpha_{22}||\alpha_{32}| \leq |\alpha_{21}||\alpha_{31}| + \sqrt{(1 - \alpha_{22}^2 - |\alpha_{21}|^2) (1 - \alpha_{33}^2 - |\alpha_{31}|^2 - |\alpha_{32}|^2)}. \quad (\text{A13})$$

The maximum of the right-hand side with respect to $|\alpha_{21}|$ and $|\alpha_{31}|$ is obtained for

$$|\alpha_{21}| = |\alpha_{31}| \sqrt{\frac{1 - \alpha_{22}^2}{1 - \alpha_{33}^2 - |\alpha_{32}|^2}}. \quad (\text{A14})$$

Substituting this value of $|\alpha_{21}|$ in (A13), after some manipulations, we obtain

$$|\alpha_{22}||\alpha_{32}| \leq \sqrt{(1 - \alpha_{22}^2) (1 - \alpha_{33}^2 - |\alpha_{32}|^2)}. \quad (\text{A15})$$

The square of this inequality leads to the constraint (7) for $|\alpha_{32}|$.

In conclusion of this Appendix, let us remark that the inequality (7) for $|\alpha_{31}|$ is weaker than the constraint (A8), that involves also $|\alpha_{32}|$, and the inequality (7) for $|\alpha_{32}|$ is weaker than the constraint (A9), that involves also $|\alpha_{21}|$, $|\alpha_{31}|$, and the relative phase between α_{32} and $\alpha_{21}^* \alpha_{31}$. Therefore, in the analyses of experimental data that involve more than one of the off-diagonal α_{ij} parameters one must use the appropriate stronger constraint.

Appendix B: Effective oscillation probabilities in SBL and LBL experiments

In this Appendix we derive the effective oscillation probabilities that are measured in the NOMAD [58] and NuTeV [59] short-baseline experiments and those that are probed in our analyses of the MINOS [62], T2K [63] and NOvA [64] long-baseline data.

Neutrino oscillation experiments that observe $\nu_\alpha \rightarrow \nu_\beta$ oscillations detect charged leptons of flavor β that are produced in a detector by a flux of neutrinos produced in a source in association with charged leptons of flavor α . In the effective three-neutrino non-unitary mixing scheme that we are considering, only the three light massive neutrinos are produced in the source. Since the effects of their sub-eV masses can be neglected in the production and detection processes, the number of ν_β events in a detector D at a distance L from a source of ν_α 's is given by[‡]

$$n_\beta^{\text{D}} = F_\beta^{\text{D}} \sigma_\beta^{\text{SM}} P_{\alpha\beta}(L) \Phi_\alpha^{\text{SM}}, \quad (\text{B1})$$

where the coefficient F_β^{D} takes into account all the quantities that characterize the detection processes (size, running time, efficiency, etc.), σ_β^{SM} is the Standard Model charged-current weak-interaction cross section for a massless ν_β , Φ_α^{SM} is the flux of Standard Model massless ν_α 's produced by the source, and $P_{\alpha\beta}(L)$ is the oscillation probability in Eq. (8). Then, the flux Φ_β^{D} of ν_β obtained from the measured number of events n_β^{D} considering the Standard Model charged-current weak-interaction cross section σ_β^{SM} is

$$\Phi_\beta^{\text{D}} = \frac{n_\beta^{\text{D}}}{F_\beta^{\text{D}} \sigma_\beta^{\text{SM}}} = P_{\alpha\beta}(L) \Phi_\alpha^{\text{SM}}. \quad (\text{B2})$$

We analyzed the MINOS data by adapting the code in the data release of Ref. [62] to the three-neutrino non-unitary mixing scheme. Since the MINOS code uses the Standard Model cross sections and the MINERvA PPFx flux [69] obtained from hadron production data only, the analysis corresponds to Eq. (B1) and the effective oscillation probability coincides with $P_{\alpha\beta}(L)$ in Eq. (8).

In the case of the T2K [63] and NOvA [64], we analyzed the far-detector (FD) ν_e and ν_μ data considering the ν_μ flux Φ_μ^{ND} measured at the near detector (ND), where the ν_μ survival probability is given by the zero-distance expression $P_{\mu\mu}^0 = ((NN^\dagger)_{\mu\mu})^2$. Hence, from Eq. (B2) the ν_β flux Φ_β^{FD} at the far detector at the distance L from the neutrino source is given by

$$\Phi_\beta^{\text{FD}} = \frac{P_{\mu\beta}(L)}{((NN^\dagger)_{\mu\mu})^2} \Phi_\mu^{\text{ND}} \quad (\beta = e, \mu). \quad (\text{B3})$$

Therefore, the effective oscillation probabilities in our analyses of the T2K and NOvA data are

$$P_{\mu\beta}^{\text{eff,LBL}} = \frac{P_{\mu\beta}(L)}{((NN^\dagger)_{\mu\mu})^2} = \frac{P_{\mu\beta}(L)}{(\alpha_{22}^2 + |\alpha_{21}|^2)^2} \quad (\beta = e, \mu). \quad (\text{B4})$$

Let us now consider the NOMAD [58] and NuTeV [59] SBL experiments, that measured the ratio of ν_e and ν_μ events in the same detector (D) at a practically zero-distance. In this case, the constraint on the appearance neutrino signal is inferred from the measured ν_μ

[‡] For simplicity, in this appendix we omit the geometrical L^{-2} flux suppression that can be added in a straightforward way.

flux and, therefore, the effective $\nu_\mu \rightarrow \nu_e$ oscillation probability is given by the ratio of the measured ν_e and ν_μ fluxes:

$$P_{\mu e}^{\text{eff,SBL}} = \frac{\Phi_e^{\text{D}}}{\Phi_\mu^{\text{D}}} = \frac{P_{\mu e}^0}{P_{\mu\mu}^0} = \frac{|(NN^\dagger)_{\mu e}|^2}{((NN^\dagger)_{\mu\mu})^2} = \frac{\alpha_{11}^2 |\alpha_{21}|^2}{(\alpha_{22}^2 + |\alpha_{21}|^2)^2}. \quad (\text{B5})$$

-
- [1] P. F. de Salas, D. V. Forero, S. Gariazzo, P. Martínez-Miravé, O. Mena, C. A. Ternes, M. Tórtola, and J. W. F. Valle, *JHEP* **21**, 071, [arXiv:2006.11237 \[hep-ph\]](#).
 - [2] F. Capozzi, E. Di Valentino, E. Lisi, A. Marrone, A. Melchiorri, and A. Palazzo, *Phys. Rev. D* **95**, 096014 (2017), [Addendum: *Phys.Rev.D* 101, 116013 (2020)], [arXiv:2003.08511 \[hep-ph\]](#).
 - [3] I. Esteban, M. Gonzalez-Garcia, M. Maltoni, T. Schwetz, and A. Zhou, *JHEP* **09**, 178, [arXiv:2007.14792 \[hep-ph\]](#).
 - [4] P. Minkowski, *Phys. Lett. B* **67**, 421 (1977).
 - [5] T. Yanagida, *Conf. Proc. C* **7902131**, 95 (1979).
 - [6] J. Schechter and J. W. F. Valle, *Phys. Rev. D* **22**, 2227 (1980).
 - [7] J. Schechter and J. W. F. Valle, *Phys. Rev. D* **25**, 774 (1982).
 - [8] R. N. Mohapatra and G. Senjanovic, *Phys. Rev. D* **23**, 165 (1981).
 - [9] R. N. Mohapatra and J. W. F. Valle, *Phys. Rev. D* **34**, 1642 (1986).
 - [10] E. K. Akhmedov, M. Lindner, E. Schnapka, and J. W. F. Valle, *Phys. Lett. B* **368**, 270 (1996), [arXiv:hep-ph/9507275](#).
 - [11] E. K. Akhmedov, M. Lindner, E. Schnapka, and J. W. F. Valle, *Phys. Rev. D* **53**, 2752 (1996), [arXiv:hep-ph/9509255](#).
 - [12] M. Malinsky, J. C. Romao, and J. W. F. Valle, *Phys. Rev. Lett.* **95**, 161801 (2005), [arXiv:hep-ph/0506296](#).
 - [13] M. Malinsky, T. Ohlsson, and H. Zhang, *Phys. Rev. D* **79**, 073009 (2009), [arXiv:0903.1961 \[hep-ph\]](#).
 - [14] M. Malinsky, T. Ohlsson, Z.-z. Xing, and H. Zhang, *Phys. Lett. B* **679**, 242 (2009), [arXiv:0905.2889 \[hep-ph\]](#).
 - [15] M. Blennow, P. Coloma, E. Fernandez-Martinez, J. Hernandez-Garcia, and J. Lopez-Pavon, *JHEP* **04**, 153, [arXiv:1609.08637 \[hep-ph\]](#).
 - [16] F. J. Escrihuela, D. V. Forero, O. G. Miranda, M. Tórtola, and J. W. F. Valle, *New J. Phys.* **19**, 093005 (2017), [arXiv:1612.07377 \[hep-ph\]](#).
 - [17] A. Atre, T. Han, S. Pascoli, and B. Zhang, *JHEP* **05**, 030, [arXiv:0901.3589 \[hep-ph\]](#).
 - [18] M. Drewes and B. Garbrecht, *Nucl. Phys. B* **921**, 250 (2017), [arXiv:1502.00477 \[hep-ph\]](#).
 - [19] D. V. Forero, S. Morisi, M. Tortola, and J. W. F. Valle, *JHEP* **09**, 142, [arXiv:1107.6009 \[hep-ph\]](#).
 - [20] S. Goswami and T. Ota, *Phys. Rev. D* **78**, 033012 (2008), [arXiv:0802.1434 \[hep-ph\]](#).
 - [21] S.-F. Ge, P. Pasquini, M. Tortola, and J. W. F. Valle, *Phys. Rev. D* **95**, 033005 (2017), [arXiv:1605.01670 \[hep-ph\]](#).
 - [22] O. G. Miranda, P. Pasquini, M. Tórtola, and J. W. F. Valle, *Phys. Rev. D* **97**, 095026 (2018), [arXiv:1802.02133 \[hep-ph\]](#).
 - [23] F. J. Escrihuela, L. J. Flores, and O. G. Miranda, *Phys. Lett. B* **802**, 135241 (2020), [arXiv:1907.12675 \[hep-ph\]](#).

- [24] O. G. Miranda, D. K. Papoulias, O. Sanders, M. Tórtola, and J. W. F. Valle, *Phys. Rev. D* **102**, 113014 (2020), [arXiv:2008.02759 \[hep-ph\]](#).
- [25] E. Fernandez-Martinez, M. B. Gavela, J. Lopez-Pavon, and O. Yasuda, *Phys. Lett. B* **649**, 427 (2007), [arXiv:hep-ph/0703098](#).
- [26] Z.-z. Xing, *Phys. Rev. D* **85**, 013008 (2012), [arXiv:1110.0083 \[hep-ph\]](#).
- [27] F. J. Escrihuela, D. V. Forero, O. G. Miranda, M. Tortola, and J. W. F. Valle, *Phys. Rev. D* **92**, 053009 (2015), [Erratum: *Phys.Rev.D* 93, 119905 (2016)], [arXiv:1503.08879 \[hep-ph\]](#).
- [28] G. C. Branco, J. T. Penedo, P. M. F. Pereira, M. N. Rebelo, and J. I. Silva-Marcos, *JHEP* **07**, 164, [arXiv:1912.05875 \[hep-ph\]](#).
- [29] A. Aguilar-Arevalo et al. (LSND), *Phys. Rev. D* **64**, 112007 (2001), [arXiv:hep-ex/0104049](#).
- [30] A. A. Aguilar-Arevalo et al. (MiniBooNE), *Phys. Rev. Lett.* **121**, 221801 (2018), [arXiv:1805.12028 \[hep-ex\]](#).
- [31] A. A. Aguilar-Arevalo et al. (MiniBooNE), *Phys. Rev. D* **103**, 052002 (2021), [arXiv:2006.16883 \[hep-ex\]](#).
- [32] J. N. Abdurashitov et al., *Phys. Rev. C* **73**, 045805 (2006), [arXiv:nucl-ex/0512041](#).
- [33] M. Laveder, *Nucl. Phys. B Proc. Suppl.* **168**, 344 (2007).
- [34] C. Giunti and M. Laveder, *Mod. Phys. Lett. A* **22**, 2499 (2007), [arXiv:hep-ph/0610352](#).
- [35] G. Mention, M. Fechner, T. Lasserre, T. A. Mueller, D. Lhuillier, M. Cribier, and A. Letourneau, *Phys. Rev. D* **83**, 073006 (2011), [arXiv:1101.2755 \[hep-ex\]](#).
- [36] C. Giunti and T. Lasserre, *Ann. Rev. Nucl. Part. Sci.* **69**, 163 (2019), [arXiv:1901.08330 \[hep-ph\]](#).
- [37] A. Diaz, C. A. Argüelles, G. H. Collin, J. M. Conrad, and M. H. Shaevitz, *Phys. Rept.* **884**, 1 (2020), [arXiv:1906.00045 \[hep-ex\]](#).
- [38] S. Böser, C. Buck, C. Giunti, J. Lesgourgues, L. Ludhova, S. Mertens, A. Schukraft, and M. Wurm, *Prog. Part. Nucl. Phys.* **111**, 103736 (2020), [arXiv:1906.01739 \[hep-ex\]](#).
- [39] A. P. Serebrov et al. (NEUTRINO-4), *Pisma Zh. Eksp. Teor. Fiz.* **109**, 209 (2019), [arXiv:1809.10561 \[hep-ex\]](#).
- [40] C. Giunti, Y. F. Li, C. A. Ternes, and Y. Y. Zhang, *Phys. Lett. B* **816**, 136214 (2021), [arXiv:2101.06785 \[hep-ph\]](#).
- [41] T. Ohlsson, C. Popa, and H. Zhang, *Phys. Lett. B* **692**, 257 (2010), [arXiv:1007.0106 \[hep-ph\]](#).
- [42] S. Parke and M. Ross-Lonergan, *Phys. Rev. D* **93**, 113009 (2016), [arXiv:1508.05095 \[hep-ph\]](#).
- [43] A. de Gouvêa and A. Kobach, *Phys. Rev. D* **93**, 033005 (2016), [arXiv:1511.00683 \[hep-ph\]](#).
- [44] O. G. Miranda, M. Tortola, and J. W. F. Valle, *Phys. Rev. Lett.* **117**, 061804 (2016), [arXiv:1604.05690 \[hep-ph\]](#).
- [45] E. Fernandez-Martinez, J. Hernandez-Garcia, and J. Lopez-Pavon, *JHEP* **08**, 033, [arXiv:1605.08774 \[hep-ph\]](#).
- [46] H. Päs and P. Sicking, *Phys. Rev. D* **95**, 075004 (2017), [arXiv:1611.08450 \[hep-ph\]](#).
- [47] I. Martinez-Soler and H. Minakata, *PTEP* **2020**, 063B01 (2020), [arXiv:1806.10152 \[hep-ph\]](#).
- [48] A. M. Coutinho, A. Crivellin, and C. A. Manzari, *Phys. Rev. Lett.* **125**, 071802 (2020), [arXiv:1912.08823 \[hep-ph\]](#).
- [49] S. A. R. Ellis, K. J. Kelly, and S. W. Li, *JHEP* **12**, 068, [arXiv:2008.01088 \[hep-ph\]](#).
- [50] K. Chakraborty, S. Goswami, and K. Long, *Phys. Rev. D* **103**, 075009 (2021), [arXiv:2007.03321 \[hep-ph\]](#).
- [51] Z. Hu, J. Ling, J. Tang, and T. Wang, *JHEP* **01**, 124, [arXiv:2008.09730 \[hep-ph\]](#).
- [52] D. Meloni, T. Ohlsson, W. Winter, and H. Zhang, *JHEP* **04**, 041, [arXiv:0912.2735 \[hep-ph\]](#).
- [53] D. Dutta, P. Ghoshal, and S. Roy, *Nucl. Phys. B* **920**, 385 (2017), [arXiv:1609.07094 \[hep-ph\]](#).

- [54] Y.-F. Li, Z.-z. Xing, and J.-y. Zhu, *Phys. Lett. B* **782**, 578 (2018), [arXiv:1802.04964 \[hep-ph\]](#).
- [55] C. Soumya and M. Rukmani, *J. Phys. G* **45**, 095003 (2018).
- [56] L. S. Miranda, P. Pasquini, U. Rahaman, and S. Razzaque, *Eur. Phys. J. C* **81**, 444 (2021), [arXiv:1911.09398 \[hep-ph\]](#).
- [57] K. J. Kelly, P. A. Machado, S. J. Parke, Y. F. Perez Gonzalez, and R. Zukanovich-Funchal, *Phys. Rev. D* **103**, 013004 (2021), [arXiv:2007.08526 \[hep-ph\]](#).
- [58] P. Astier et al. (NOMAD), *Phys. Lett. B* **570**, 19 (2003), [arXiv:hep-ex/0306037](#).
- [59] S. Avvakumov et al. (NuTeV), *Phys. Rev. Lett.* **89**, 011804 (2002), [arXiv:hep-ex/0203018](#).
- [60] P. Astier et al. (NOMAD), *Nucl. Phys. B* **611**, 3 (2001), [arXiv:hep-ex/0106102](#).
- [61] E. Eskut et al. (CHORUS), *Nucl. Phys. B* **793**, 326 (2008), [arXiv:0710.3361 \[hep-ex\]](#).
- [62] P. Adamson et al. (MINOS+), *Phys. Rev. Lett.* **122**, 091803 (2019), [arXiv:1710.06488 \[hep-ex\]](#).
- [63] K. Abe et al. (T2K), *Phys. Rev. D* **103**, 112008 (2021), [arXiv:2101.03779 \[hep-ex\]](#).
- [64] Alex Himmel, *New Oscillation Results from the NOvA Experiment* (2020).
- [65] Patrick Dunne, *Latest Neutrino Oscillation Results from T2K* (2020).
- [66] M. Acero et al. (NOvA), *Phys. Rev. D* **98**, 032012 (2018), [arXiv:1806.00096 \[hep-ex\]](#).
- [67] P. Huber, M. Lindner, and W. Winter, *Comput. Phys. Commun.* **167**, 195 (2005), [arXiv:hep-ph/0407333 \[hep-ph\]](#).
- [68] P. Huber, J. Kopp, M. Lindner, M. Rolinec, and W. Winter, *Comput. Phys. Commun.* **177**, 432 (2007), [arXiv:hep-ph/0701187 \[hep-ph\]](#).
- [69] L. Aliaga et al. (MINERvA), *Phys. Rev. D* **94**, 092005 (2016), [Addendum: *Phys. Rev. D* **95**, 039903 (2017)], [arXiv:1607.00704 \[hep-ex\]](#).
- [70] G. Barenboim, C. A. Ternes, and M. A. Tórtola, *JHEP* **07**, 155, [arXiv:2005.05975 \[hep-ph\]](#).
- [71] S. S. Chatterjee and A. Palazzo, *Phys. Rev. Lett.* **126**, 051802 (2021), [arXiv:2008.04161 \[hep-ph\]](#).
- [72] P. B. Denton, J. Gehrlein, and R. Pestes, *Phys. Rev. Lett.* **126**, 051801 (2021), [arXiv:2008.01110 \[hep-ph\]](#).